ESC European Society of Cardiology

Cardiovascular Research (2019) **115**, 1861–1872
doi:10.1093/cvr/cvz068

Pentraxin 3 deficiency protects from the metabolic inflammation associated to diet-induced obesity

Fabrizia Bonacina[1†], Annalisa Moregola[1†], Rémi Porte[2], Andrea Baragetti[1,3], Eduardo Bonavita[4], Alice Salatin[1], Liliana Grigore[3,5], Fabio Pellegatta[3,5], Martina Molgora[2], Marina Sironi[2], Elisa Barbati[2], Alberto Mantovani[2,6], Barbara Bottazzi[2], Alberico Luigi Catapano[1,5]*, Cecilia Garlanda[2,6], and Giuseppe Danilo Norata[1,3]*

[1]Department of Excellence of Pharmacological and Biomolecular Sciences, Università degli Studi di Milano, Via Balzaretti 9, 20133 Milan, Italy; [2]IRCC Humanitas Clinical and Research Center, Rozzano, Italy; [3]Centro SISA per lo Studio dell'Aterosclerosi, Ospedale Bassini, Cinisello Balsamo, Italy; [4]Cancer Inflammation and Immunity Group, CRUK Manchester Institute, The University of Manchester, Manchester M20 4BX, UK; [5]IRCSS Multimedica, Milan, Italy; and [6]Humanitas University Rozzano, Italy

Received 1 August 2018; revised 23 January 2019; editorial decision 4 March 2019; accepted 11 March 2019; online publish-ahead-of-print 12 March 2019

Time for primary review: 23 days

This manuscript was handled by consulting editor, Federica Marelli-Berg.

Aims Low-grade chronic inflammation characterizes obesity and metabolic syndrome. Here, we aim at investigating the impact of the acute-phase protein long pentraxin 3 (PTX3) on the immune-inflammatory response occurring during diet-induced obesity.

Methods and results PTX3 deficiency in mice fed a high-fat diet for 20 weeks protects from weight gain and adipose tissue deposition in visceral and subcutaneous depots. This effect is not related to changes in glucose homeostasis and lipid metabolism but is associated with an improved immune cell phenotype in the adipose tissue of *Ptx3* deficient animals, which is characterized by M2-macrophages polarization and increased angiogenesis. These findings are recapitulated in humans where carriers of a *PTX3* haplotype (*PTX3* h2/h2 haplotype), resulting in lower PTX3 plasma levels, presented with a reduced prevalence of obesity and decreased abdominal adiposity compared with non-carriers.

Conclusion Our results support a critical role for PTX3 in the onset of obesity by promoting inflammation and limiting adipose tissue vascularization and delineate PTX3 targeting as a valuable strategy for the treatment of adipose tissue-associated inflammatory response.

Keywords Pentraxin 3 • Inflammed adipose tissue • Immunometabolism

1. Introduction

Obesity is an epidemic condition leading to health complications such as diabetes and cardiovascular diseases.[1] Obesity, which is frequently the consequence of nutrient excess and loss of metabolic homeostasis, contributes to a state of chronic low-grade inflammation,[2] which results in an increase of systemic pro-inflammatory mediators and the switch of adipose tissue resident immune cells from a tolerogenic to a pro-inflammatory phenotype.[3]

Adipose tissue-resident immune cells, once activated, produce adipokines and cytokines, including tumour necrosis factor α (TNFα), interleukin-1β (IL-1β), interleukin-6 (IL-6), and C-C Motif Chemokine Ligand 2 (Ccl2), thus supporting the recruitment of new immune cells that perpetuate the local and systemic state of inflammation.[4,5] Although increased circulating levels of C-reactive protein (CRP) parallels the development of obesity and metabolic syndrome,[6] the behaviour of other acute phase proteins, as the long pentraxin 3 (PTX3), in such conditions is still elusive.

* Corresponding authors. Tel: +39 02 50318302-401; fax: +39 02 50318386, E-mail: alberico.catapano@unimi.it (A.L.C.); Tel: +39 02 50318313; fax: +39 02 50318386, E-mail: Danilo.Norata@unimi.it (G.D.N.)

† The first two authors contributed equally to the study.

PTX3 is a homo-octameric secreted glycoprotein which shares the C-terminal domain with CRP and serum amyloid P component (both short pentraxins), and possesses a unique and unrelated N-terminal domain, which accounts for PTX3-specific functions.[7] Similar to CRP, PTX3 is induced by inflammatory signals, such as IL-1β,[7] TNFα,[8] and microbe-associate molecular patterns,[9] but synthetized by several cells types, including myeloid-derived cells,[10] vascular endothelial cells,[11] smooth muscle cells,[12] and also adipocytes.[8] PTX3 activates innate immune responses by interacting with some pathogen moieties and complement components (C1q, Ficolins, Factor H),[13] thus promoting the phagocytosis of some microorganism, and tuning inflammatory responses. Moreover, PTX3 modulate vascular biology by dampening neutrophils recruitment to inflammatory sites[14] and reactivity through P-selectin binding,[15] reducing arterial thrombosis,[16] atherosclerosis,[17] and the size of myocardial infarction.[18]

In humans, PTX3 plasma levels rapidly increase few hours after myocardial infarction[19] and are an independent predictor of 3-month mortality.[20] More recently, increased PTX3 plasma levels have been associated with multifactorial inflammatory diseases, including endothelial dysfunction and advanced vascular inflammation in diabetes,[21] non-alcoholic fatty liver disease,[22] and chronic kidney disease.[23]

Genetically obese (ob/ob) and obese-diabetic (db/db) mice present higher levels of *Ptx3* mRNA in visceral adipose tissue (VAT) compared with lean mice, an effect consistent with increased levels of TNFα.[8] In humans, PTX3 is produced by adipocytes in VAT and subcutaneous adipose tissue (SCAT)[24,25] and its levels in VAT have been associated with macrophages infiltration in obese subjects but not in controls.[24] These findings are reflected in the direct association of PTX3 plasma levels with metabolic syndrome[26] and obesity[27] a finding that however is not consistent in all cohorts.[28,29]

Thus to elucidate whether PTX3, a key molecule linking innate immunity, inflammation and obesity,[24,30,31] represents a bystander or plays an active role in the immunoinflammatory response observed during obesity, we profiled the immunoinflammatory and metabolic response to an obesogenic diet of *Ptx3*$^{-/-}$ compared with wild type (WT) littermates and investigated in humans the impact of a *PTX3* haplotype[32–34] on ectopic fat deposition and metabolic status.

2. Methods

2.1 Animals

WT and *Ptx3*$^{-/-}$ male mice littermates on the C57BL/6 genetic background were bred in house and generated as in detail described previously.[35] C57BL/6 WT mice for the first crossings were from Charles River Italy. Homozygous mutant mice display female subfertility due to abnormalities of the cumulus oophorus and are susceptible to invasive pulmonary aspergillosis associated with defective recognition of conidia by alveolar macrophages and dendritic cells and impaired induction of adaptive Type 2 responses (http://www.informatics.jax.org/marker/MGI:104641). Eight-week old mice were housed four per cages and kept in a temperature-controlled environment (20 ± 2°C, 50 ± 5% relative humidity) with a 12-h light/dark cycle in an air-conditioned room and free access to food and water. Starting from 8 weeks of age, male littermates WT and *Ptx3*$^{-/-}$ mice were randomized in two groups, one fed a standard fat diet (SFD, 10% Kcal from fat, Research diet INC, Cat#D12450H), and one an high-fat diet (HFD, 45% Kcal from fat, Research diet INC, Cat#D12451). Food intake and weight gain were measured weakly. Mice were sacrificed at 20 weeks, after isoflurane (2%) inhalation and cervical dislocation, and VAT, SCAT, brown adipose tissue (BAT), liver, and blood were collected and weighted. All animal procedures performed conform to the guidelines from directive 2010/63/EU of the European Parliament on the protection of animals used for scientific purposes and were approved by the Ethical Committee (Progetto di Ricerca 2012/02, Autorizzazione Ministeriale 811/2017).

2.2 Magnetic resonance for imaging

Magnetic resonance for imaging (MRI) was used to evaluate VAT, SCAT, and BAT depots in WT and *Ptx3*$^{-/-}$ mice on HFD diet. For this procedure, mice were anaesthetized with 2% isoflurane. Consecutive photos at the level of shoulder blades, chest, and abdomen of each mouse were acquired and subsequently analysed with Photoshop® software for the quantification of adipose tissue deposition.

2.3 Glucose and insulin tolerance test

Intraperitoneal glucose tolerance test (IP-GTT) and insulin tolerance test (ITT) were used to measure plasmatic clearance of glucose after intraperitoneal injection of glucose or insulin respectively. In brief, animals were fasted overnight (approximately 14 h), then blood glucose levels at fasting and after 15, 30, 60, 90, and 120 min from injection of glucose solution (20% w/v in PBS, 2 mg per grams of body weight) were measured with a glucometer (ONE-TOUCH Ultra glucometer). For ITT, the animals were fasted for 4 h. Glucose plasma levels were measured at fasting and after 15, 30, 60, 90, and 120 min from injection of human recombinant insulin (1 mU per gram of body weight, Humulin R100 Ul/mL).

2.4 Samples preparation for immunophenotyping by flow cytometry

Fresh collected blood was stained (50 µL) after the lysis of red blood cells with ACK solution ($KHCO_3$ 10 mM, NH_4Cl 150 mM, EDTA 0.1 mM) for 10 min at room temperature.

Fresh VAT and SCAT were placed on ice in a six well plate and cut in small pieces in 2 mL of PBS 5% BSA solution, then collagenase (2 mg/mL final concentration, NB4 standard grade, Serva) and $CaCl_2$ (5 mM final concentration) were added and samples were incubated at 37°C for 40 min under agitation. Samples were then top up with MACS (PBS, 2% FCS, 2 mM EDTA) and filtered on a sterile bandage and subsequently on a 100 µm and 70 µm cells strainer. After the lysis of red blood cells with ACK for 5 min on ice, samples were washed, spin and resuspended in 50 µL of antibodies mix (Supplementary material online, *Table S1*). All flow cytometry antibodies were used at 1:100 dilutions unless otherwise specified, optimal antibody concentrations for staining were calculated based on manufacturer instructions.

For immunophenotyping a cell suspension containing 1×10^6 cells or 50 µL of blood were acquired with FACS Calibur (BD Bioscience) or Novocyte 3000 (ACEA Biosciences). Cell sorting was performed with FACSAria II flow cytometer (BD Bioscience). Antibodies used are listed in the Supplementary material online, *Table S1*.

2.5 Blood biochemistry measurements

Blood samples were collected in EDTA tubes by tail vein at 10 weeks and intracardiac puncture at 20 weeks and plasma was separated by centrifugation (8000 rcf for 10 min) at 4°C.

Total plasma cholesterol and triglycerides were measured from frozen plasma by standard enzymatic techniques using the Cholesterol CP KIT (ABX Pentra, HORIBA Medical) or the triglyceride CP KIT (ABX Pentra, HORIBA Medical). Cholesterol and triglyceride concentration were read by spectrophotometer at 490 nm (Bio-Rad iMark microplate

reader). Plasma insulin concentrations were quantified using mouse Ultrasensitive ELISA kit (Mercodia).

PTX3 plasma levels in human blood samples at enrolment were determined as previously described[36] with sandwich ELISA (detection limit 0.1 ng/mL, inter-assay variability from 8% to 10%) developed in-house, by personnel blind to patients' characteristics. Data are reported as ng/mL.

2.6 Histology

Part of the VAT and SCAT was fixed overnight in 4% buffer formalin (Sigma-Aldrich), embedded in paraffin and tissue section (5μm) stained with haematoxylin and eosin (Sigma-Aldrich). Haematoxylin/eosin stained sections from the adipose tissue of each animal were acquired using the axiovision Zeiss software (a field of 0.2 mm^2 at 10× of magnification). Quantification of adipocytes areas was performed using Adobe Photoshop software: an area with intact adipocytes was manually selected, then the calculated area (1 pixel = 0.6289 micron) was divided for the number of adipocytes counted in that selected area (at least four independent measurement per mouse). Crown-like structures were counted from eight visceral sections per mouse ($n = 6$) by an operator blinded of the genotypes.

Immunofluorescence analysis of WT and *Ptx3*$^{-/-}$ VAT were performed by staining with F4/80 antibody (Biolegend), to identify crown-like structure, and CD31 antibody (Abcam) for the identification of the vasculature.

2.7 Quantitative real time PCR (qRT-PCR)

Total RNA from cells and VAT was isolated using Nucleo Spin RNA kit (Machery NAGEL) and RNAsi Lipid Tissue Mini kit (QIAGEN), respectively, as indicated in the manufacturer instruction.

RNA assessed for quality and quantity using absorption measurements (NanoDrop™ 1000 Spectrophotometer, Thermo Fisher Scientific) and reverse transcribed into cDNA (400 ng RNA) with iScriptTM cDNA synthesis kit (BioRad). Gene expression analysis was performed with SYBR Green Supermix (ThermoFisher Scientific) in CFX connect light cycler (BioRad, Cat#1708841). Expression was calculated using the ΔΔCt method (Livak and Schmittgen, 2001) and normalized to a housekeeping gene (*Rpl*, L Ribosomal Protein). Primers for qPCR were designed with the help of online tools (https://www.eurofinsgenomics.eu/). The thermal cycling profile was a two-step amplification (95°C for 5 min, followed by 45 cycles of 95°C for 10 s and 55°C for 30 s). The sequences of the qPCR Primers are reported in the Supplementary material online, *Table S2*.

2.8 Immunoblotting

Adipose tissue was homogenized in RIPA buffer (0.1% sodium dodecyl sulfate, 0.5% sodium deoxycholate, 1% Nonidet P-40, 150 mM NaCl, and 50 mM Tris HCl, pH 8.0, supplemented with protease inhibitors). Tissues were lysed at 4°C for 15 min and clarified by centrifugation at 12 000 rcf. Lysates were separated by SDS-PAGE transferred to nitrocellulose and immunoblot with primary antibody (anti-VEGF 'Vascular Endothelial Growth Factor' Biorbyt orb256347, anti-CD31 'Cluster of Differentiation 31' Cell Signaling 77699 and anti-α Tubulin, Sigma-Adrich T5168) followed by HRP-conjugated secondary antibodies. HRP activity was identify by enhanced chemiluminescence (Clarity Western ECL, BioRad) and Odyssey Imaging System.

2.9 *In vitro* macrophages differentiation

Murine bone marrow-derived macrophages (BMDM) were generated collecting cells from both mouse femurs. Red blood cells from this preparation were lysed with 100 μL ACK solution for 2 min at room temperature. The cells were then cultured 24 h on 75 cm^2 culture flask. Non-adherent cells (2.5×10^6 cells/well) were cultured in a 12 wells plate, 6 days in D-MEM, 10% FBS with 20 ng/mL recombinant murine (rm) M-CSF (Peprotech) changing the medium every 3 days. One day before polarization, growth medium was replaced by D-MEM, 10% FBS. Cells were cultured for 6 h with 100 ng/mL LPS purified from *Escherichia coli* 055:B5 (sigma-Aldrich) plus 20 ng/mL rmIFNg (Peprotech) for M1 polarization, 20 ng/mL rmIL-4 (Peprotech) to induce M2 polarization or only in D-MEM, 10% FBS, M0 condition. Human recombinant PTX3 was used at 200 ng/mL.

2.10 Human study—anthropometric measurements

Measurements of body composition and regional adipose tissue distribution was performed via dual-energy X-ray absorptiometry (DEXA), as previously described,[37] using a Lunar iDXA (Ge Healthcare, Madison, WI, USA). Scans were then analysed through enCORE software (version 14.0), in order to set regions of interest for detection and quantification, discriminating among bone mass (calculating density as well), lean and adipose tissue. Android fat was computed automatically over the android region, a region-of-interest automatically defined by the enCORE software, whose caudal limit is automatically placed at the top of the iliac crest and whose height is set to 20% of the distance from the top of the iliac crest to the base of the skull to define its cephalad limit. The investigation is conform to the principles outlined in the Declaration of Helsinki. Each subject signed the informed consent for the collection of blood samples and clinical data for research purposes prior to the inclusion in the study.

2.11 Statistical analysis

Statistical analysis was performed using Prism (GraphPad) and SPSS v.23 (IBM Corp., Chicago, IL, USA) for human data. Both mice and human data are expressed as mean ± SEM and a *P*-value of less than 0.05 was considered significant (*$P < 0.05$, **$P < 0.01$, and ***$P < 0.001$). For comparison between two groups an unpaired two-sides test with a 95% confidence interval was used. In detail, for groups with more than seven observations, after checking for the normal distribution of data, a parametric Student's *t*-test was applied, whereas for groups with less than six observations or not normally distributed a Mann–Whitney non-parametric test was used, as also indicated in the figure legends. For human data, Mann–Whitney and Kolmogorov–Smirnov non-parametric test were used to compare anthropometric variables and plasma PTX3 levels after testing the distribution of the groups using the Shapiro–Wilk test.

3. Results

3.1 PTX3 level increases during high-fat diet feeding and supports the development of obesity

Adipose tissue expansion associates with a worsening of the inflammatory status both locally and systemically.[38] Therefore, we first investigated whether plasma levels of PTX3 change during the onset of obesity, as an index of innate response activation. To this aim, WT mice were fed

a HFD or a SFD for 20 weeks. As expected, HFD-fed mice showed increased body weight and increased VAT and SCAT deposition (Supplementary material online, *Figure S1A* and *B*). Moreover, HFD-fed mice displayed an impaired glucose tolerance and insulin sensitivity as assessed by GTT and ITT (Supplementary material online, *Figure S1C* and *D*). HFD mice also presented an increased infiltration of monocytes and macrophages into the VAT, which associated to increased *Ccl2* and *Cd68* mRNA expression (Supplementary material online, *Figure S1E* and *F*). In agreement with the increased immune-inflammatory profile, PTX3 plasma levels were also significantly increased after 10 and 20 weeks of HFD feeding compared with SFD feeding (*Figure 1A*).

This observation prompted us to investigate whether PTX3 plays a causal role or simply reflects the underlying inflammatory response associated to obesity. Therefore, WT and *Ptx3*$^{-/-}$ mice were fed up to 20 weeks with HFD. PTX3 deficiency was associated with significant reduced weight gain compared with WT (*Figure 1B*), in spite of a similar daily food intake (Supplementary material online, *Figure S2A*). This phenotype was confirmed by MRI analysis showing a reduced VAT and SCAT deposition at both 10 and 20 weeks of HFD in *Ptx3*$^{-/-}$ mice compared with WT mice (*Figure 1C–E*); whereas the amount of BAT in the intrascapular area was similar between the two experimental groups (*Figure 1E* and Supplementary material online, *Figure S2B* and *C*). At sacrifice, the amount of VAT and SCAT but not of BAT was significantly reduced in *Ptx3*$^{-/-}$ mice compared with WT mice. Similar weights for liver, pancreas, and spleen were also observed (*Figure 1E*).

These data suggest that PTX3 plays a non-redundant role during HFD-induced obesity and brought us to explore whether the phenotype observed might have been the consequence of impaired glucose metabolism. To this end, we measured basal glycaemia following overnight fasting and performed an intraperitoneal glucose (IP-GTT) and ITT in WT and *Ptx3*$^{-/-}$ mice after 10 and 20 weeks of diet. Basal glycaemia was similar between WT and *Ptx3*$^{-/-}$ mice following 10-week or 20-week of HFD (WT 121 ± 10 mg/dL, *Ptx3*$^{-/-}$ 111 ± 9 mg/dL at 10 weeks; WT 145 ± 13 mg/dL, *Ptx3*$^{-/-}$ 130 ± 3 mg/dL at 20 weeks, respectively), as were glucose curves over time after IP-GTT or ITT (*Figure 2A–D*). Likewise, plasma insulin levels and lipid profile were not different between *Ptx3*$^{-/-}$ and WT mice after 20-week HFD (*Figure 2E–G*). Similarly, data collected in mice fed a SFD showed a comparable metabolic profile (analysis of body weight, glucose, and insulin tolerance) between WT and *Ptx3*$^{-/-}$ mice (Supplementary material online, *Figure S3A–E*).

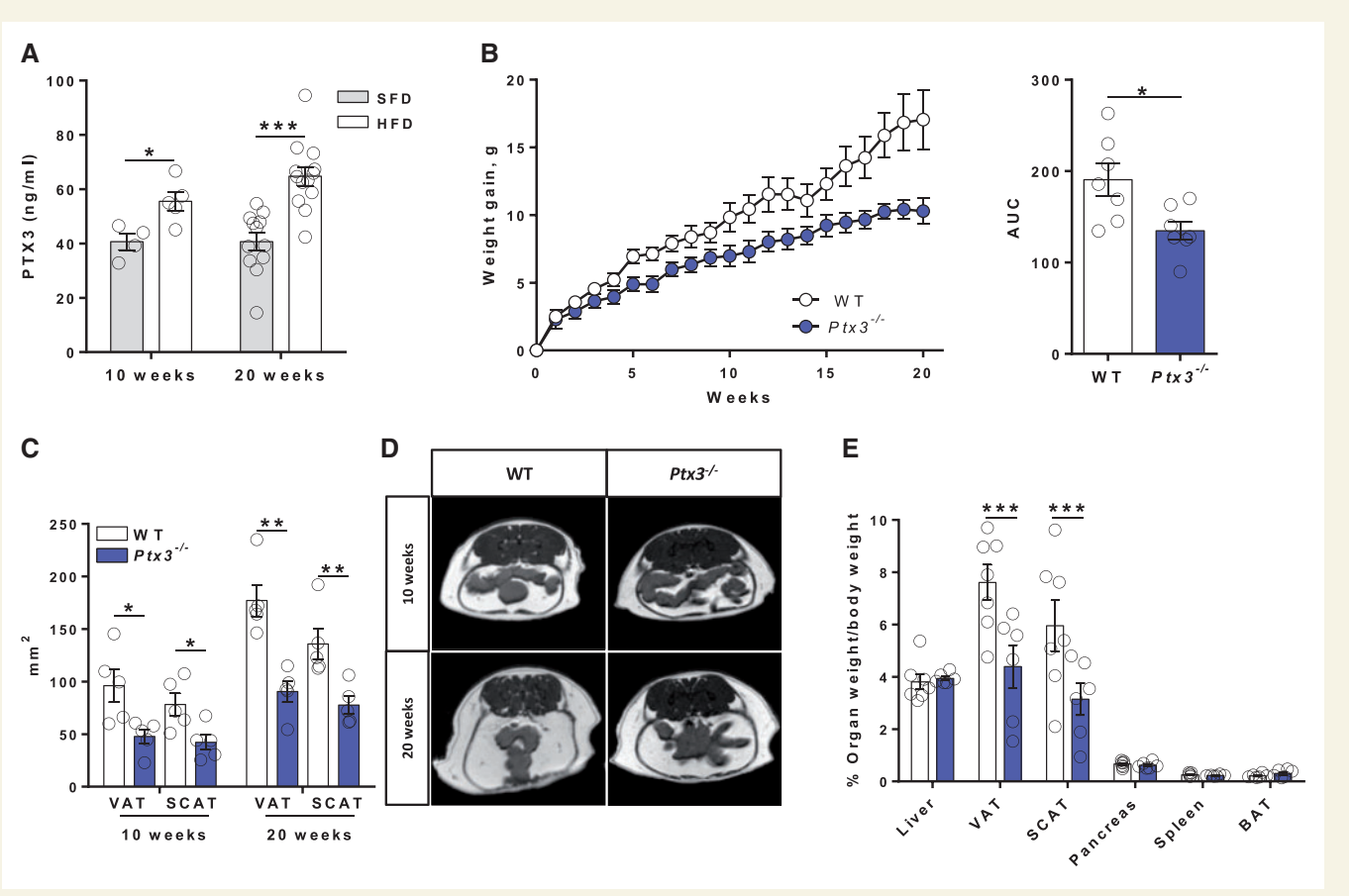

Figure 1 PTX3 is implicated in diet-induced obesity. (*A*) Plasma PTX3 levels measured at 10 weeks ($n = 4–5$ per group) and 20 weeks ($n = 12–13$ per group) after the starting of the high-fat diet (HFD) in C57BL/6 mice. (*B*) Weight gain of WT and *Ptx3*$^{-/-}$ mice on HFD measured weekly and area under the curve (AUC) of weight gain, $n = 7$ per group. (*C*) Visceral (VAT) and subcutaneous (SCAT) adipose tissues in WT and *Ptx3*$^{-/-}$ mice on HFD evaluated by magnetic resonance imaging (MRI). Analysis was performed at 10 weeks (left) and 20 weeks (right) of HFD feeding, $n = 5$ per group. (*D*) Representative pictures of magnetic resonance imaging of data presented in *C*. (*E*) Percentage of organ weight compared with final body weight at 20 week HFD, $n = 6–7$ per group. Data are presented as mean ± SEM. Statistical analysis was performed with Student's *t*-test (*A*, *B*, *F*) or Mann–Whitney test (*A*, *C*, *E*), $^*P < 0.05$, $^{**}P < 0.01$.

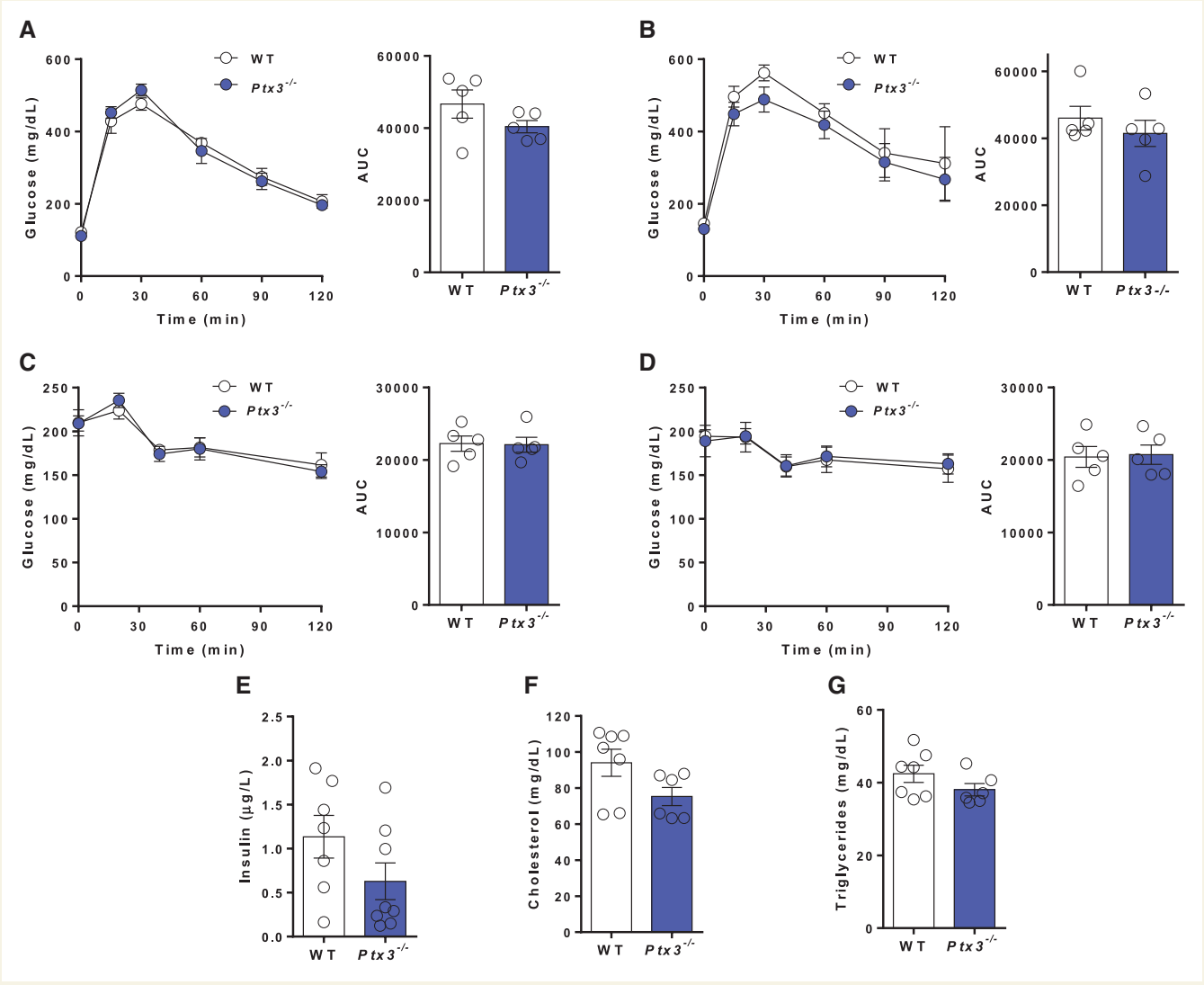

Figure 2 PTX3 deficiency does not affect glucose homeostasis and lipid metabolism during diet-induced obesity. (*A* and *B*) Glucose tolerance test (GTT) performed at 10 (*A*) and 20 (*B*) weeks of HFD feeding in WT and *Ptx3*$^{-/-}$ mice, $n = 5$ per group. Glycaemia was measured before i.p. glucose injection ($t = 0$, baseline values) and after 15, 30, 60, 90, and 120 min. (*C* and *D*) Insulin tolerance test (ITT) performed at 10 (*C*) and 20 (*D*) weeks of HFD feeding in WT and PTX3 KO mice, $n = 5$ per group. Glycaemia was measured before i.p. insulin injection ($t = 0$, baseline values) and after 20, 40, 60, and 120 min. (*E*–*G*) Insulin (*E*), cholesterol (*F*), and triglycerides (G) plasma concentrations in WT and PTX3 plasma, $n = 6$–8 per group. Data are presented as mean ± SEM. Statistical analysis was performed with Student's *t*-test (*E*) or Mann–Whitney test (*A*–*D*, *F*, *G*).

All together these results ruled out that a conserved glucose and lipid homeostasis explains the phenotype of *Ptx3*$^{-/-}$ mice, and therefore, point to other mechanisms of protection to HFD-induced obesity.

3.2 PTX3 deficiency promotes pro-resolution macrophage skewing

Next, we investigated whether the decreased weight gain and fat accumulation might have been related to a different inflammatory profile in *Ptx3*$^{-/-}$ mice. First, we profiled circulating immune cell signature in *Ptx3*$^{-/-}$ and WT mice on HFD (*Figure 3*). A significant decrease in the number of circulating neutrophils was observed (457 ± 39 cells/µL and 350 ± 35 cells/µL for WT and *Ptx3*$^{-/-}$ mice, respectively, $P < 0.05$; *Figure 3B*), while the absolute count of blood monocytes was similar between WT and *Ptx3*$^{-/-}$ fed a HFD (322 ± 36 cells/µL and 266 ± 36 cells/µL for WT and *Ptx3*$^{-/-}$ mice, respectively, data not shown) as was the case for monocytes subsets distribution (*Figure 3C*). The number of circulating CD3^{+} T and CD19^{+} B lymphocytes (CD3^{+}: WT = 741 ± 196 cells/µL and KO = 643 ± 115 cells/µL; CD19^{+}: WT = 3040 ± 656 cells/µL and KO = 2495 ± 403 cells/µL, data not shown) and distribution of the different CD4^{+} and CD8^{+} T cells subsets (Tnaive, Tcentral and effector memory, T effector cells) was also similar between WT and *Ptx3*$^{-/-}$ mice (*Figure 3D*–*G*). A similar immune profile was observed in *Ptx3*$^{-/-}$ and WT mice fed a SFD (Supplementary material online, *Figure S4A*–*G*).

Despite of a similar circulating leucocytes frequency, the analysis of the inflammatory profile in the VAT and SCAT of HFD-fed *Ptx3*$^{-/-}$ mice showed a decreased expression of markers associated with inflammation, such as *Ccl2* and *Il6*, compared with WT mice (*Figure 4A* and Supplementary material online, *Figure S5A*). This profile was associated with a significant reduction in the number of monocytes, macrophages, and neutrophils that accumulate in the VAT of *Ptx3*$^{-/-}$ mice compared with WT (*Figure 4B*, see also Supplementary material online, *Figure S6* for

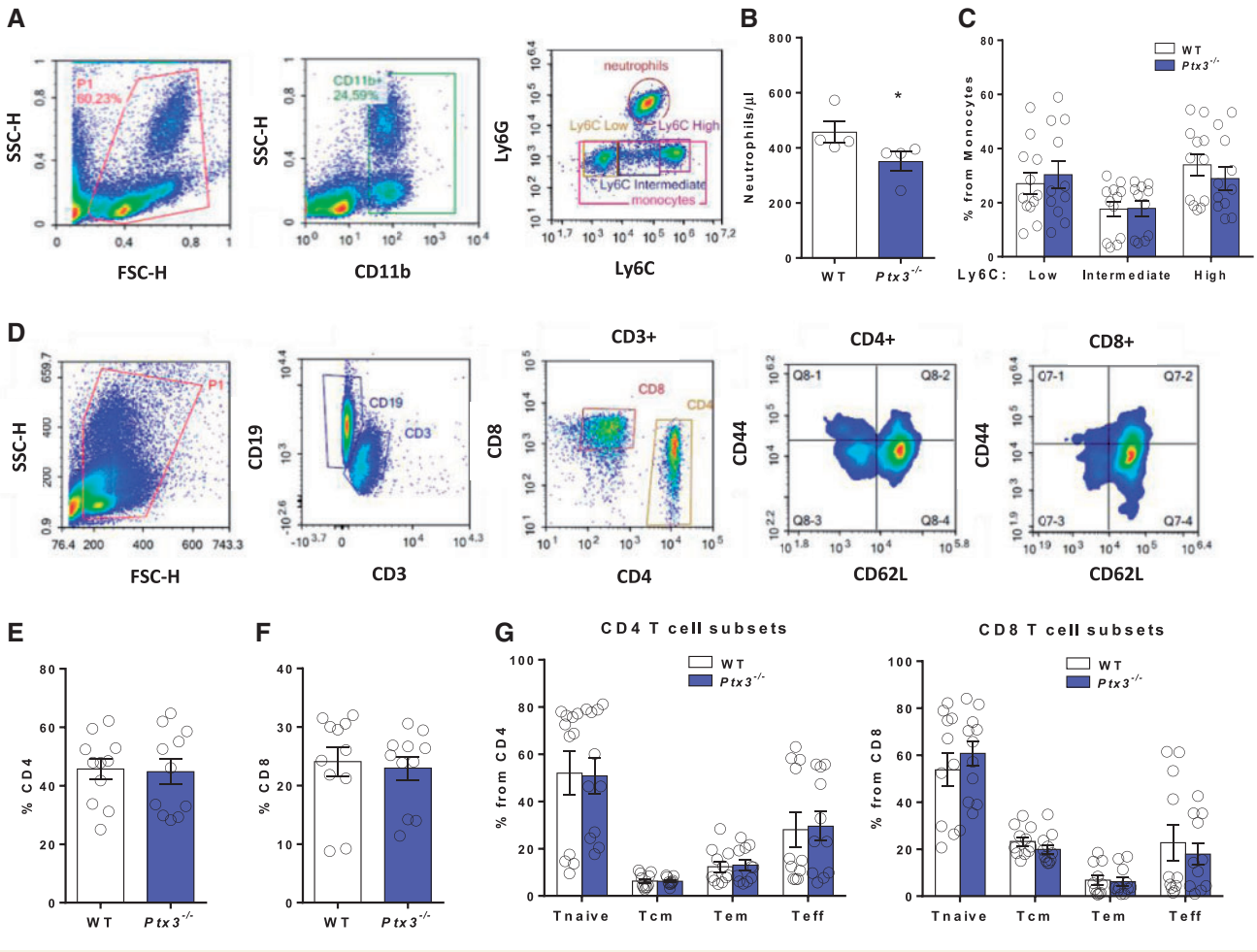

Figure 3 Protection to HFD-induced obesity of *Ptx3*$^{-/-}$ mice is not the consequence of a different circulating immune signature. (*A*) Gating strategy for the identification of monocytes (CD11b+Ly6C+Ly6G-) and neutrophils (CD11b+Ly6G+) in the blood of WT and *Ptx3*$^{-/-}$ mice from flow cytometry analysis. (*B*) Neutrophils/µL of blood in WT and *Ptx3*$^{-/-}$ mice on HFD, $n = 4$ per group. (*C*) Analysis of monocytes subsets in blood of WT and *Ptx3*$^{-/-}$ mice on HFD, $n = 11$–12 per group. (*D*) Gating strategy for the identification of B cells (CD19+CD3-), T cells (CD19-CD3+, T helper CD4+, T cytotoxic CD8+), and T cells subsets in blood of WT and *Ptx3*$^{-/-}$ mice (T naive—Tn CD62L+CD44-, T effector memory—Tem CD62-CD44+, T central memory—Tcm CD62L+CD44+, T effector—Teff CD62-CD44-) from flowcytometry analysis. (*D*–*F*) Percentages of CD4+ (*E*) and CD8+ (*F*) T lymphocytes and their subsets (*G*) in blood of WT and *Ptx3*$^{-/-}$ mice, $n = 11$ per group. Data are presented as mean ± SEM. Statistical analysis was performed with Student's *t*-test (*C*, *E*–*G*) or Mann–Whitney test (*B*).

gating strategy). Differently, only macrophage number was reduced in SCAT of *Ptx3*$^{-/-}$ mice compared with WT (Supplementary material online, *Figure S5B*). In addition, the phenotypic characterization of monocytes and macrophages isolated from the VAT revealed that monocytes from *Ptx3*$^{-/-}$ VAT presented a reduced expression of *Ccr2* (CCL2 receptor) but not of *Cx3cr1* (CX3CL1 or Fractalkine receptor, marker highly expressed on alternative activated monocytes) compared with WT (*Figure 4C*), pointing towards a pro-resolving profile of monocytes. In parallel, *Ptx3*$^{-/-}$ VAT macrophages presented a significant increased expression of *Arg1* (Arginase 1) and *Ym1* (M2-like molecules) compared with WT macrophages (*Figure 4D*). This difference was specific for VAT macrophages but not for macrophages infiltrating the SCAT (Supplementary material online, *Figure S5C*). Next, we assessed whether PTX3 affects macrophage polarization. *Ptx3*$^{-/-}$ M0 BMDM, present an increased expression of *Ym1, Arg1*, and *Ifng* (*Figure 4E*); incubation of M1 BMDM from WT and *Ptx3*$^{-/-}$ mice with recombinant PTX3 results in increased expression of *Il6* and a decrease of *Ym1* and *Cd206* expression (*Figure 4F*). These data further support the ability of PTX3 to sustain an M1 response.

In agreement with the reduced inflammatory profile, macrophage count, and consequently, the frequency of crown-like structures surrounding dying or dead adipocytes, where macrophages resorb the remnants of these dying cells,[39] was significantly decreased in *Ptx3*$^{-/-}$ VAT (*Figure 4G and H* and Supplementary material online, *Figure S7*). These results suggest that PTX3 deficiency associates with lower monocytes recruitment and macrophages M1-polarization in VAT.

3.3 Enhanced vascularization limits visceral adipose hypertrophy in *Ptx3*$^{-/-}$ mice

Obesity associates with hypertrophic visceral adipocytes that, undergoing cell death, promote an inflammatory response.[38] Physiological adipose tissue expansion is controlled by the rate of vascularization and angiogenesis that plays a crucial role favouring a correct oxygen supply

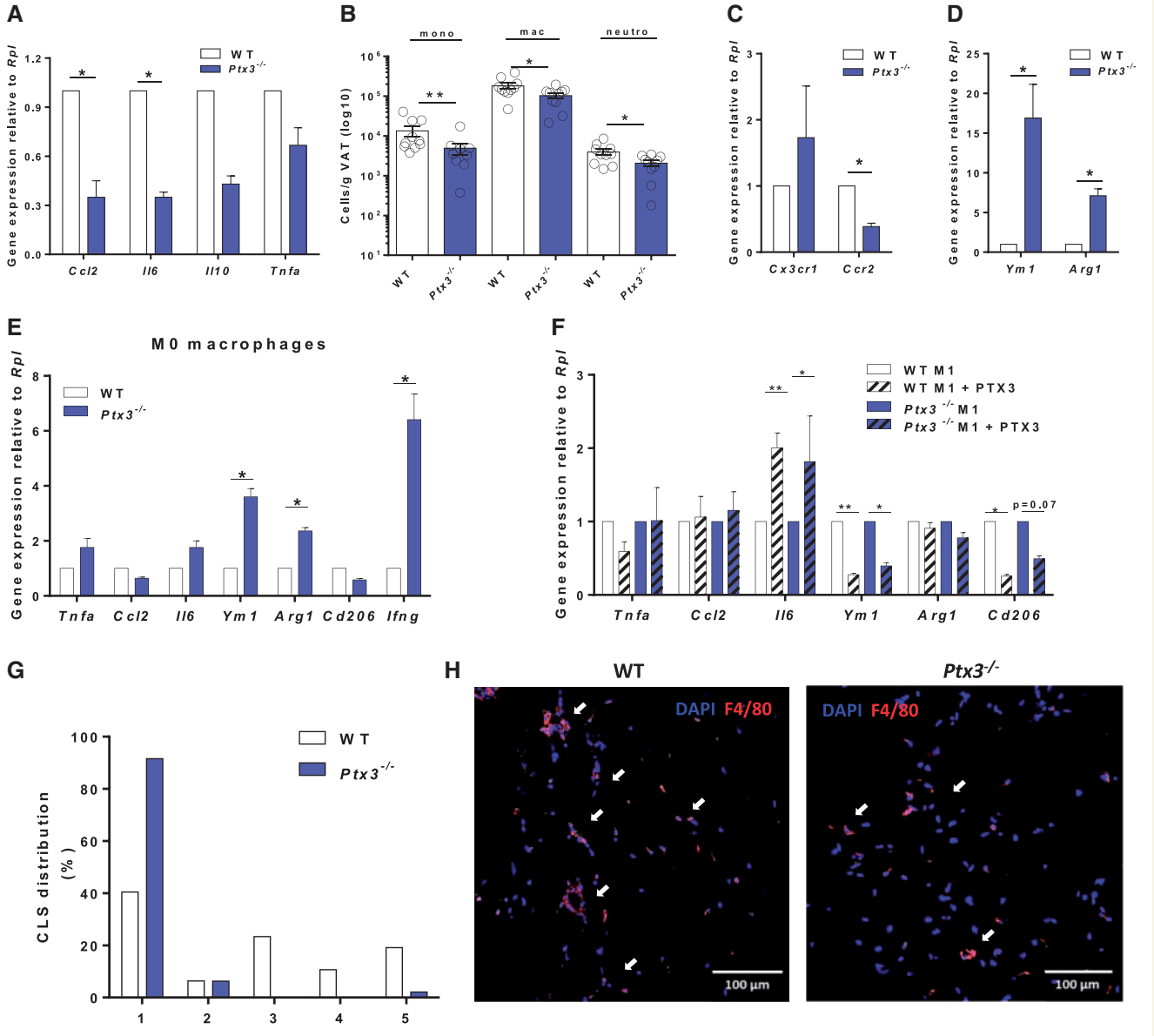

Figure 4 PTX3 deficiency is associated with reduced inflammation and innate immune cells recruitment in VAT. (*A*) mRNA expression relative to *Rpl* (L Ribosomal Protein) of inflammatory genes in VAT of WT and *Ptx3*$^{-/-}$ mice on 20-week HFD, $n = 5–10$ per group. (*B*) Numbers corrected for tissue weight of sorted monocytes (mono), macrophages (mac), and neutrophils (neutro) in VAT, $n = 9–10$ per group, of WT and *Ptx3*$^{-/-}$ on 20-week HFD. (*C* and *D*) mRNA expression relative to *Rpl* in monocytes (*C*) and macrophages (*D*) sorted from VAT of WT and *Ptx3*$^{-/-}$ mice on 20-week HFD, $n = 3–5$ per group. (*E*) mRNA expression relative to *Rpl* (L Ribosomal Protein) of M0, M1, and M2 macrophages from WT and *Ptx3*$^{-/-}$ mice differentiated *in vitro* for 6 h, $n = 5–6$ per group. (*F*) Effect of exogenous rhPTX3 on mRNA expression in M1 BMDM from *Ptx3*$^{-/-}$ and WT mice, $n = 4–8$ per group. (*G*) Quantification of the numbers of crown-like structures in VAT sections from WT and *Ptx3*$^{-/-}$ mice on 20-week HFD (legends: from score 1, no crown detected, to score 5, equal or more than 4 crowns), $n = 6$ per group. (*H*) Representative images of crown-like structures in VAT of WT and *Ptx3*$^{-/-}$ mice stained with F4/80 antibody. Data are presented as mean ± SEM. Statistical analysis was performed with Student's *t*-test (*A*, *B*) or Mann–Whitney test (*A*, *C–F*), $^{*}P < 0.05$, $^{**}P < 0.01$.

to adipocytes. Accordingly, we found that adipocytes from *Ptx3*$^{-/-}$ VAT (*Figure 5A*) and SCAT (Supplementary material online, *Figure S8A*) displayed a reduced hypertrophy compared with WT mice. Given the anti-angiogenetic role of PTX3, accomplished by binding and thus inhibiting fibroblast growth factor 2 (FGF2),[40,41] we investigated whether PTX3 deficiency impairs adipose tissue vascularization, assessing the expression of key markers of angiogenesis. As shown in *Figure 5B Cd31* and *Vegfa* (vascular endothelial growth factor a), mRNA expression was significantly increased in VAT from *Ptx3*$^{-/-}$ compared with that from WT mice. Concordantly, VEGFA protein expression and VAT vascularization were increased in *Ptx3*$^{-/-}$ mice compared with WT animals (*Figure 5C–F*). This effect appeared to be independent of macrophage-derived VEGF as its expression was similar in M0, M1 or M2 macrophages from WT or *Ptx3*$^{-/-}$ BMDM (Supplementary material online, *Figure S8B*). In addition,

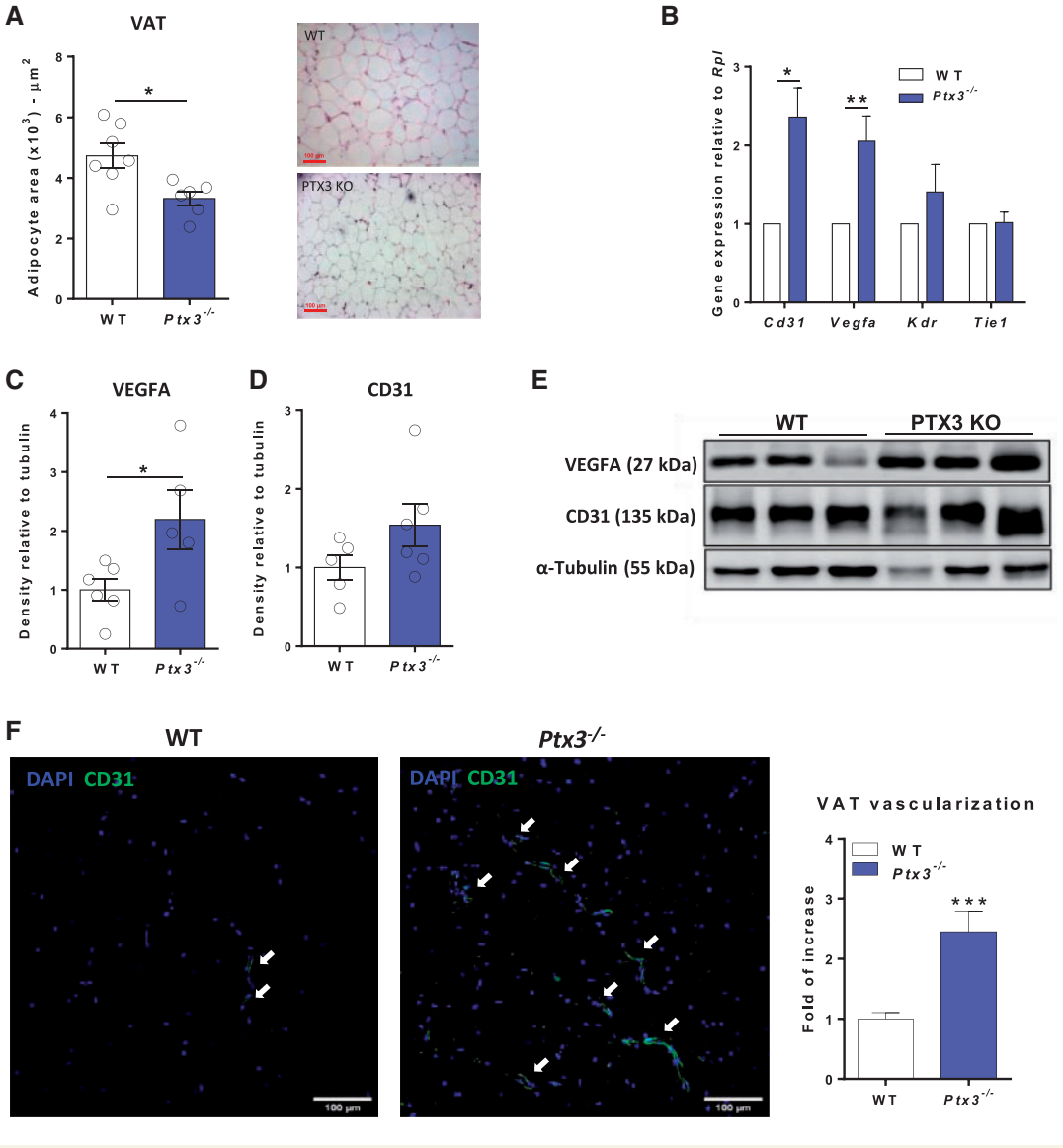

Figure 5 *Ptx3*$^{-/-}$ mice present smaller adipocytes and an enhanced VAT vascularization. (*A*) Quantification of adipocyte area in VAT of WT and *Ptx3*$^{-/-}$ on 20-week HFD, $n = 6–7$ per group; representative pictures of sections stained with haematoxylin and eosin are shown. (*B*) mRNA expression relative to *Rpl* (L Ribosomal Protein) of genes related to vascularization in VAT of WT and *Ptx3*$^{-/-}$ mice on 20-week HFD, $n = 6–8$ per group. (*C* and *D*) Quantification of VEGFA (*C*) and CD31 (*D*) in VAT of WT and *Ptx3*$^{-/-}$ mice on 20-week HFD, $n = 5–6$ per group. (*E*) Representative panel for VEGFA (27 kDa) and CD31 (135 kDa) western blot are shown. Data are presented as mean ± SEM. (*F*) Quantification of vasculature by CD31 staining in *Ptx3*$^{-/-}$ and WT VAT. Statistical analysis was performed with Student's *t*-test (*B*, *F*) or Mann–Whitney test (*A*, *C*, *D*), $^{*}P < 0.05$, $^{**}P < 0.01$.

the expression of angiogenic factors was similar in the SCAT of WT or *Ptx3*$^{-/-}$ mice (Supplementary material online, *Figure S8C*), thus suggesting that PTX3 deficiency results in less pronounced inflammatory profile and enhanced angiogenesis in the VAT.

3.4 Genetic determined lower PTX3 levels in humans relates with a reduced visceral adipose tissue accumulation

To translate our findings in humans, we investigated whether the presence of two different haplotypes (h1/h1 vs h2/h2) on the PTX3 locus,[34] which result in lower PTX3 levels, associated with a different metabolic profile. The carriers of the h2/h2 haplotype ($n = 817$) showed significant lower PTX3 plasma levels compared with subjects with the h1/h1 haplotype ($n = 163$) [h1/h1 median 3.65 ng/mL (3.13, 4.15); h2/h2 median 3.47 (3.07, 3.96)] (*Figure 6A*), which was associated with a significant lower body mass index [h1/h1 median 27.45 kg/m^2 (25, 30.09); h2/h2 median 26.6 kg/m^2 (24.25, 29.41)] (*Figure 6B*). We next measured adipose tissue accumulation by DEXA (*Figure 6C*) and observed that subjects with the h2/h2 haplotype also presented a significant reduction in adipose tissue accumulation in the android area (an index of visceral adiposity) [h1/h1 median 48.35% (42.25, 52.88); h2/h2 median 46.70% (39.65, 52.95)](*Figure 6D*) but a similar distribution in the gynoid area (an index of subcutaneous adiposity) [h1/h1 median 42.30% (32.65, 52.03); h2/h2 median 44.20% (33.60, 51.90)] (*Figure 6E*), resulting in a significant difference in android-gynoid ratio [h1/h1 median 1.12 (0.98, 1.35); h2/h2

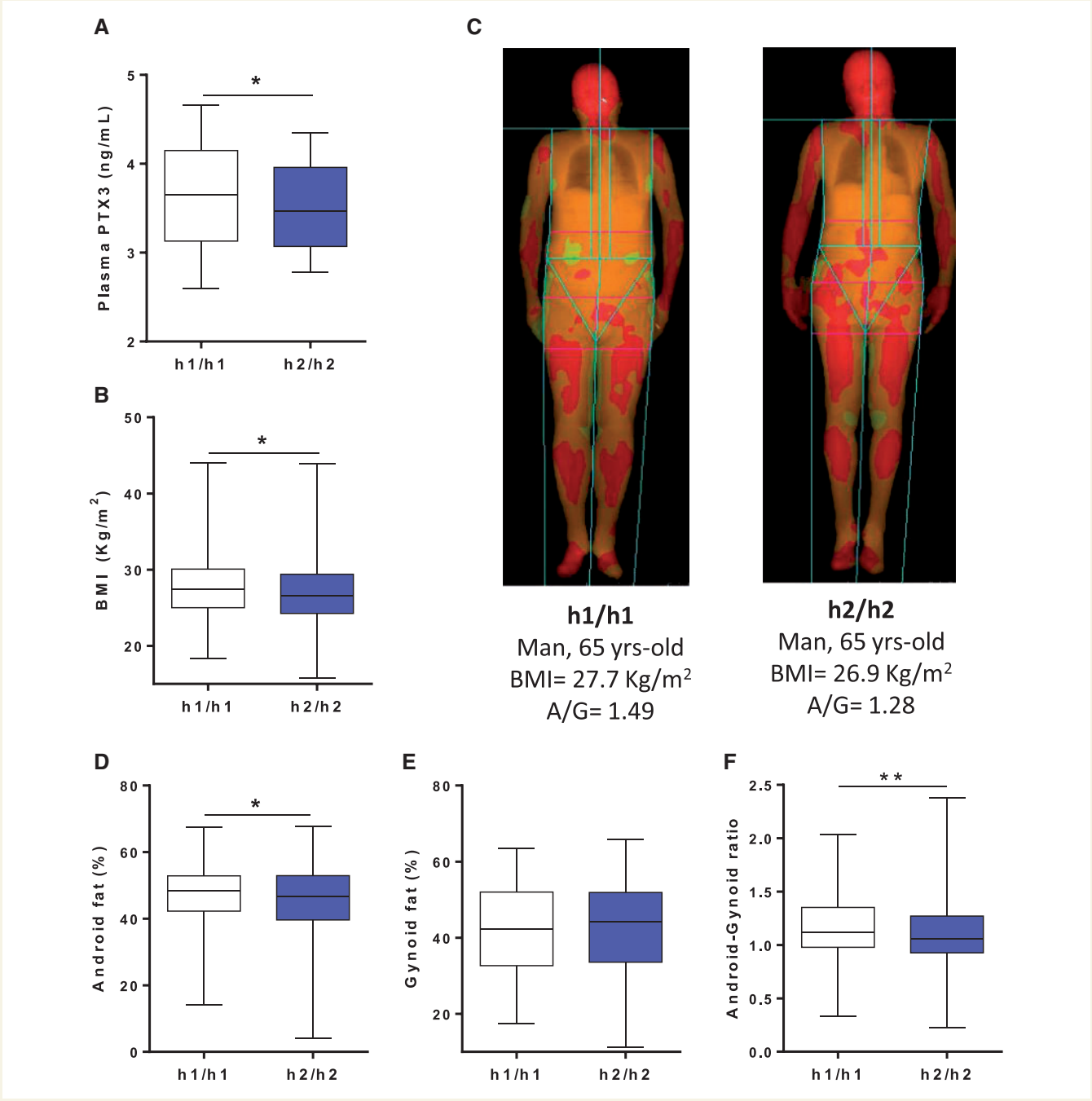

Figure 6 Carriers of the h2/h2 PTX3 haplotype present reduced PTX3 plasma levels, Body mass index (BMI), and visceral fat accumulation. (*A*) PTX3 plasma levels in h1/h1 and h2/h2 subjects from the PLIC study cohort; h1/h1, $n = 163$, h2/h2, $n = 817$. (*B*) BMI, h1/h1 ($n = 201$), h2/h2 ($n = 921$). (*C*) Representative images obtained by dual-energy X-ray absorption (DEXA) scan of two individuals of the h1/h1 and h2/h2 haplotypes carriers for PTX3. (*D*) Android fat mass and (*E*) gynoid fat mass were evaluated by DEXA scan in the two groups, h1/h1 ($n = 210$), h2/h2 ($n = 921$). (*F*) Android-gynoid ration. Data are presented as mean ± SEM, Statistical analysis was performed with Kolmogorov–Smirnov test (*A*), Mann–Whitney test (*B*, *D*–*F*), $^{*}P < 0.05$, $^{**}P < 0.01$.

median 1.06 (0.93, 1.27)] (*Figure 6F*). These data extended the observations in animal models supporting the relevance of PTX3 on indexes of obesity also in humans.

4. Discussion

This work demonstrates that PTX3 deficiency reduces the development of obesity by controlling the immunoinflammatory response and the grade of vascularization in VAT (*Figure 7*). The translation to humans further confirms that carriers of a PTX3 haplotype, whose PTX3 plasma levels are reduced, present decreased adipose tissue accumulation.

Healthy AT behaves as a pool of 'anti-inflammatory', 'pro-resolving', and long-lived memory immune cells.[42] Excessive accumulation of fat, as a result of over nutrition and increased circulating levels of free fatty acids, however, prompts an inflammatory response, which is paralleled by the infiltration of activated effector immune cells in AT,[43] and by a

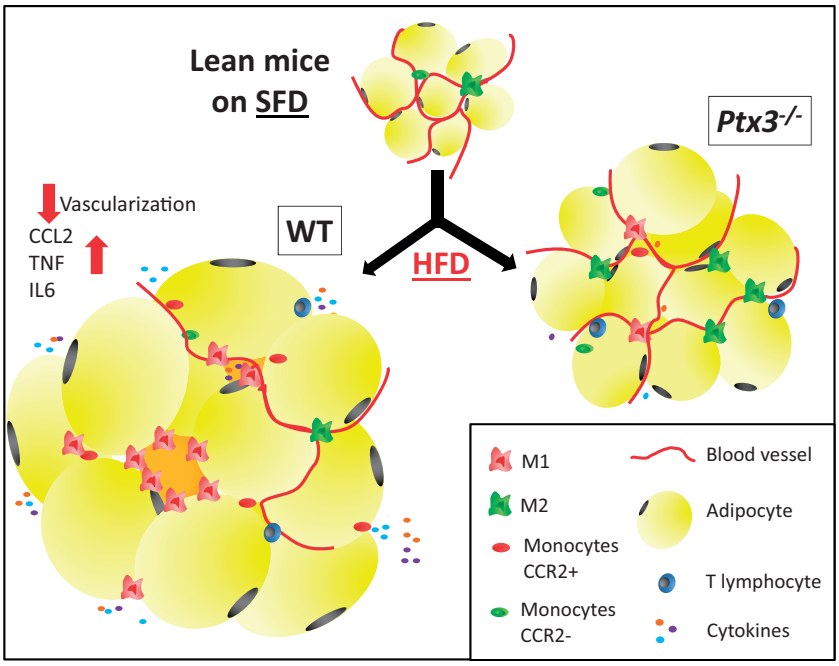

Figure 7 PTX3 deficiency protects from HFD-induced obesity. PTX3 deficiency associates with less pronounced visceral adipose tissue hypertrophy. This effect is associated with increased vascularization, decreased infiltration of pro-inflammatory monocytes and macrophages.

systemic increased of circulating activated immune cells,[44] which further support adipose-tissue inflammation and insulin resistance. Whether this inflammatory response follows or contributes to adipocyte hypertrophy is still a matter of discussion, but it is recognized that the improvement of the immunoinflammatory responses counteracts the metabolic complications associated with obesity. Indeed, deficiency of CCL2, a key chemoattractant protein, reduces macrophage accumulation in adipose tissue, insulin resistance, and hepatic steatosis associated with obesity,[45] while the blockade of the costimulatory molecule CD40 and its signalling intermediates, TNF receptor-associated factors 6 (TRAF6), ameliorates insulin resistance, and hepatosteatosis by reducing CD8+ T cell infiltration into adipose tissue.[46] Similarly, our data show that PTX3 deficiency preserves the M2-like phenotype of adipose tissue macrophages thus preventing fat accumulation and inflammation during HFD-induced obesity. PTX3 is a member of the pentraxin family, soluble mediators of innate immune arm, whose levels rapidly increase following an inflammatory insult.[31] Whereas CRP accurately reflects the inflammatory state associated to obesity,[6] PTX3 appears to play a role in modulating the immune response in different contexts[31]: by limiting neutrophils recruitment,[14] protecting from atherosclerosis[17] and thrombosis,[16] decreasing cardiac necrosis[18] and platelet-leucocyte aggregation after myocardial infarction,[15] reducing restenosis[40] and fibrotic scar formation,[47] and behaving as onco-suppressor.[48] On the other hand, PTX3 has been also involved in promoting inflammation after intestinal ischaemia and reperfusion.[49] All these evidences delineate the complex role of PTX3 that might depend on cell/tissue origin and can be affected by the glycosylation variability of the N-terminal domain.[50]

Furthermore, PTX3 deficiency was shown to result in increased M2 macrophage polarization in the context of experimental models of mesenchymal and epithelial carcinogenesis, thus favouring protumoral immune responses and increased tumour growth.[48] PTX3 was also demonstrated to control angiogenesis and vascularization by binding to FGF2 and inhibiting its angiogenic function.[40] Angiogenesis is a complex process, which exerts different functions based on the physiopathological mechanism in which it is involved. Angiogenesis is detrimental in atherosclerosis where it contributes to plaque growth and instability,[51] while its promotion in adipose tissue by angiogenetic factors, such as VEGF and FGF2 (secreted by both adipocytes and activated macrophages) favours the delivery of oxygen and nutrients to adipocytes,[52] thus preventing hypoxia caused by adipocyte hypertrophy, as a consequence of excessive fat accumulation.[53] Moreover, a direct correlation between VEGF expression, adipose tissue vascularization and the M2 macrophage activation was shown.[54,55] Of note, maintenance of an M2 phenotype has been associated with a metabolic healthy adipose tissue,[56] whereas the prevalence of M1-like macrophages, primarily found in crown-like structures (CLSs) around dying adipocytes,[39] associates to the development of an inflamed adipose tissue during obesity.

These aspects point to the hypothesis that the improved profile observed in VAT from *Ptx3*$^{-/-}$ mice could depend on both the prevalence of M2 macrophages as well as increased vascularization. Indeed, we observed that PTX3 deficiency protects from adipose tissue expansion during high fat induced-obesity through the maintenance of an anti-inflammatory milieu, mainly as the consequence of the prevalence of M2-macrophages. Moreover, we demonstrated that PTX3 deficiency is accompanied by increased CD31 and VEGF expression in adipose tissue thus indicating the presence of an improved vascular network which might also contribute to reduced fat accumulation in *Ptx3*$^{-/-}$ mice. Of note, VEGF was already shown to be a targetable strategy for the prevention of obesity promoting vessel blood formation and M2-polarization.[54] Which could be the molecular mechanism beyond the improved M2 polarization under PTX3 deficient conditions? PTX3, when bound to pathogens, interacts with C1q and favours complement activation; vice versa fluid-phase PTX3 sequesters

C1q, thus dampening its activity.[57] Of note C1q was shown to modulate macrophage polarization towards M2 phenotype independently from complement activation.[58] These findings suggest to further explore whether, at the molecular level, the effect of PTX3 could be the consequence of the modulation of soluble factors such as C1q, directly implicated in macrophage polarization.

Considering that PTX3 shares a 82% sequence similarity between mouse and man,[7] we next investigated whether the findings in animal models might be translated to humans.

We extend previous findings showing that PTX3 plasma levels mark the immunoinflammatory response associated to obesity,[26] by demonstrating that specific genetic settings which were found to alter PTX3 plasma levels in Ghanaian women[32] and in lung-transplant recipients with primary graft dysfunction[33] result in significant lower body mass index and reduced visceral fat accumulation, further suggesting a direct connection between lower genetically determined PTX3 plasma levels and improved metabolic profile in humans.

These data, together with the observation in animal models, indicate that PTX3 might contribute to obesity development by limiting adipose tissue vascularization and promoting macrophage infiltration. As a consequence, although the inhibition of PTX3 might be beneficial for the treatment of obesity, the other protective effects associated to PTX3[31,48] suggest the need for the development of tissue selective PTX3 targeting strategies to fully exploit its pharmacological potential.

Supplementary material

Supplementary material is available at *Cardiovascular Research* online.

Authors' contributions

Conceived and designed the experiments: G.D.N., F.B., A.Mo., A.L.C., B.B., C.G., A.M. Performed the experiments: F.B., A.Mo., R.P., A.B., E.B., A.S., L.G., F.P., M.M., E.B., M.S. Analysed the data: F.B., A.Mo., R.P., A.B., G.D.N. Wrote the paper: F.B., A.M., R.P., G.D.N. Revised the paper for scientific content: F.B., A.Mo., R.P., B.B., C.G., A.L.C., G.D.N.

Acknowledgements

The help of Federico Simone Colombo for technical assistance during cell sorting is kindly acknowledged.

Conflict of interest: none declared.

Funding

This work was supported by the Fondazione Cariplo [2015-0524 to A.L.C., 2015-0564 to A.M. and A.L.C. and 2016-0852 to G.D.N.]; H2020 REPROGRAM [PHC-03-2015/667837-2 to A.L.C.]; Ministero della Salute [GR-2011-02346974 to G.D.N. and GR-2013-02355011 to F.B.]; Cluster Alisei [MEDINTECH CTN01_00177_962865 to A.M.]; European Commission, ERC project [PHII-669415 to A.M.]; Ministero dell'Istruzione, dell'Università e della Ricerca (MIUR), PRIN project [2015YYKPNN to A.M.]; and the XXXI cycle of Graduate School in Experimental and Clinical Pharmacological Sciences of the Università degli Studi di Milano (to A.Mo.).

References

1. Wilson PW, D'Agostino RB, Sullivan L, Parise H, Kannel WB. Overweight and obesity as determinants of cardiovascular risk: the Framingham experience. *Arch Intern Med* 2002;**162**:1867–1872.
2. Hotamisligil GS. Inflammation, metaflammation and immunometabolic disorders. *Nature* 2017;**542**:177–185.
3. Lumeng CN, Bodzin JL, Saltiel AR. Obesity induces a phenotypic switch in adipose tissue macrophage polarization. *J Clin Invest* 2007;**117**:175–184.
4. Hotamisligil GS, Shargill NS, Spiegelman BM. Adipose expression of tumor necrosis factor-alpha: direct role in obesity-linked insulin resistance. *Science* 1993;**259**:87–91.
5. Ruscica M, Baragetti A, Catapano AL, Norata GD. Translating the biology of adipokines in atherosclerosis and cardiovascular diseases: gaps and open questions. *Nutr Metab Cardiovasc Dis* 2017;**27**:379–395.
6. Aronson D, Bartha P, Zinder O, Kerner A, Markiewicz W, Avizohar O, Brook GJ, Levy Y. Obesity is the major determinant of elevated C-reactive protein in subjects with the metabolic syndrome. *Int J Obes* 2004;**28**:674–679.
7. Breviario F, d'Aniello EM, Golay J, Peri G, Bottazzi B, Bairoch A, Saccone S, Marzella R, Predazzi V, Rocchi M. Interleukin-1-inducible genes in endothelial cells. Cloning of a new gene related to C-reactive protein and serum amyloid P component. *J Biol Chem* 1992;**267**:22190–22197.
8. Abderrahim-Ferkoune A, Bezy O, Chiellini C, Maffei M, Grimaldi P, Bonino F, Moustaid-Moussa N, Pasqualini F, Mantovani A, Ailhaud G, Amri EZ. Characterization of the long pentraxin PTX3 as a TNFalpha-induced secreted protein of adipose cells. *J Lipid Res* 2003;**44**:994–1000.
9. Introna M, Alles VV, Castellano M, Picardi G, De Gioia L, Bottazzai B, Peri G, Breviario F, Salmona M, De Gregorio L, Dragani TA, Srinivasan N, Blundell TL, Hamilton TA, Mantovani A. Cloning of mouse ptx3, a new member of the pentraxin gene family expressed at extrahepatic sites. *Blood* 1996;**87**:1862–1872.
10. Doni A, Peri G, Chieppa M, Allavena P, Pasqualini F, Vago L, Romani L, Garlanda C, Mantovani A. Production of the soluble pattern recognition receptor PTX3 by myeloid, but not plasmacytoid, dendritic cells. *Eur J Immunol* 2003;**33**:2886–2893.
11. Norata GD, Marchesi P, Pirillo A, Uboldi P, Chiesa G, Maina V, Garlanda C, Mantovani A, Catapano AL. Long pentraxin 3, a key component of innate immunity, is modulated by high-density lipoproteins in endothelial cells. *Arterioscler Thromb Vasc Biol* 2008;**28**:925–931.
12. Klouche M, Peri G, Knabbe C, Eckstein HH, Schmid FX, Schmitz G, Mantovani A. Modified atherogenic lipoproteins induce expression of pentraxin-3 by human vascular smooth muscle cells. *Atherosclerosis* 2004;**175**:221–228.
13. Deban L, Jarva H, Lehtinen MJ, Bottazzi B, Bastone A, Doni A, Jokiranta TS, Mantovani A, Meri S. Binding of the long pentraxin PTX3 to factor H: interacting domains and function in the regulation of complement activation. *J Immunol* 2008;**181**:8433–8440.
14. Deban L, Russo RC, Sironi M, Moalli F, Scanziani M, Zambelli V, Cuccovillo I, Bastone A, Gobbi M, Valentino S, Doni A, Garlanda C, Danese S, Salvatori G, Sassano M, Evangelista V, Rossi B, Zenaro E, Constantin G, Laudanna C, Bottazzi B, Mantovani A. Regulation of leukocyte recruitment by the long pentraxin PTX3. *Nat Immunol* 2010;**11**:328–334.
15. Maugeri N, Rovere-Querini P, Slavich M, Coppi G, Doni A, Bottazzi B, Garlanda C, Cianflone D, Maseri A, Mantovani A, Manfredi AA. Early and transient release of leukocyte pentraxin 3 during acute myocardial infarction. *J Immunol* 2011;**187**:970–979.
16. Bonacina F, Barbieri SS, Cutuli L, Amadio P, Doni A, Sironi M, Tartari S, Mantovani A, Bottazzi B, Garlanda C, Tremoli E, Catapano AL, Norata GD. Vascular pentraxin 3 controls arterial thrombosis by targeting collagen and fibrinogen induced platelets aggregation. *Biochim Biophys Acta* 2016;**1862**:1182–1190.
17. Norata GD, Marchesi P, Pulakazhi Venu VK, Pasqualini F, Anselmo A, Moalli F, Pizzitola I, Garlanda C, Mantovani A, Catapano AL. Deficiency of the long pentraxin PTX3 promotes vascular inflammation and atherosclerosis. *Circulation* 2009;**120**:699–708.
18. Salio M, Chimenti S, De Angelis N, Molla F, Maina V, Nebuloni M, Pasqualini F, Latini R, Garlanda C, Mantovani A. Cardioprotective function of the long pentraxin PTX3 in acute myocardial infarction. *Circulation* 2008;**117**:1055–1064.
19. Peri G, Introna M, Corradi D, Iacuitti G, Signorini S, Avanzini F, Pizzetti F, Maggioni AP, Moccetti T, Metra M, Cas LD, Ghezzi P, Sipe JD, Re G, Olivetti G, Mantovani A, Latini R. PTX3, A prototypical long pentraxin, is an early indicator of acute myocardial infarction in humans. *Circulation* 2000;**102**:636–641.
20. Latini R, Maggioni AP, Peri G, Gonzini L, Lucci D, Mocarelli P, Vago L, Pasqualini F, Signorini S, Soldateschi D, Tarli L, Schweiger C, Fresco C, Cecere R, Tognoni G, Mantovani A; Lipid Assessment Trial Italian Network (LATIN) Investigators. Prognostic significance of the long pentraxin PTX3 in acute myocardial infarction. *Circulation* 2004;**110**:2349–2354.
21. Katakami N, Kaneto H, Sakamoto F, Takahara M, Irie Y, Fujisawa K, Miyashita K, Yasuda T, Matsuoka TA, Yoshiuchi K, Sakamoto K, Kuroda A, Matsuhisa M, Kosugi K, Shimomura I. Plasma pentraxin 3 levels are associated with carotid IMT in type 1 diabetic patients. *Diabetes Res Clin Pract* 2013;**99**:185–191.
22. Gurel H, Genc H, Celebi G, Sertoglu E, Cicek AF, Kayadibi H, Ercin CN, Dogru T. Plasma pentraxin-3 is associated with endothelial dysfunction in non-alcoholic fatty liver disease. *Eur Rev Med Pharmacol Sci* 2016;**20**:4305–4312.
23. Baragetti A, Norata GD. Long pentraxin PTX3 as a prognostic marker of cardiovascular mortality in patients with chronic kidney disease. *Pol Arch Intern Med* 2017;**127**:152–153.
24. Alberti L, Gilardini L, Zulian A, Micheletto G, Peri G, Doni A, Mantovani A, Invitti C. Expression of long pentraxin PTX3 in human adipose tissue and its relation with cardiovascular risk factors. *Atherosclerosis* 2009;**202**:455–460.

25. Osorio-Conles O, Guitart M, Chacón MR, Maymo-Masip E, Moreno-Navarrete JM, Montori-Grau M, Näf S, Fernandez-Real JM, Vendrell J, Gómez-Foix AM. Plasma PTX3 protein levels inversely correlate with insulin secretion and obesity, whereas visceral adipose tissue PTX3 gene expression is increased in obesity. *Am J Physiol Endocrinol Metab* 2011;**301**:E1254–E1261.
26. Zanetti M, Bosutti A, Ferreira C, Vinci P, Biolo G, Fonda M, Valente M, Cattin L, Guarnieri G, Barazzoni R. Circulating pentraxin 3 levels are higher in metabolic syndrome with subclinical atherosclerosis: evidence for association with atherogenic lipid profile. *Clin Exp Med* 2009;**9**:243–248.
27. Miyaki A, Maeda S, Yoshizawa M, Misono M, Sasai H, Shimojo N, Tanaka K, Ajisaka R. Is pentraxin 3 involved in obesity-induced decrease in arterial distensibility? *J Atheroscler Thromb* 2010;**17**:278–284.
28. Ogawa T, Kawano Y, Imamura T, Kawakita K, Sagara M, Matsuo T, Kakitsubata Y, Ishikawa T, Kitamura K, Hatakeyama K, Asada Y, Kodama T. Reciprocal contribution of pentraxin 3 and C-reactive protein to obesity and metabolic syndrome. *Obesity* 2010;**18**:1871–1874.
29. Yamasaki K, Kurimura M, Kasai T, Sagara M, Kodama T, Inoue K. Determination of physiological plasma pentraxin 3 (PTX3) levels in healthy populations. *Clin Chem Lab Med* 2009;**47**:471–477.
30. Violi F, Pastori D. Pentraxin 3—a link between obesity, inflammation and vascular disease? *Circ J* 2016;**80**:327–328.
31. Bonacina F, Baragetti A, Catapano AL, Norata GD. Long pentraxin 3: experimental and clinical relevance in cardiovascular diseases. *Mediators Inflamm* 2013;**2013**: 725102.
32. May L, Kuningas M, van Bodegom D, Meij HJ, Frolich M, Slagboom PE, Mantovani A, Westendorp RG. Genetic variation in pentraxin (PTX) 3 gene associates with PTX3 production and fertility in women. *Biol Reprod* 2010;**82**:299–304.
33. Diamond JM, Meyer NJ, Feng R, Rushefski M, Lederer DJ, Kawut SM, Lee JC, Cantu E, Shah RJ, Lama VN, Bhorade S, Crespo M, Demissie E, Sonett J, Wille K, Orens J, Weinacker A, Weill D, Arcasoy S, Shah PD, Belperio JA, Wilkes D, Ware LB, Palmer SM, Christie JD; Lung Transplant Outcomes Group. Variation in PTX3 is associated with primary graft dysfunction after lung transplantation. *Am J Respir Crit Care Med* 2012;**186**:546–552.
34. Cunha C, Aversa F, Lacerda JF, Busca A, Kurzai O, Grube M, Loffler J, Maertens JA, Bell AS, Inforzato A, Barbati E, Almeida B, Santos e Sousa P, Barbui A, Potenza L, Caira M, Rodrigues F, Salvatori G, Pagano L, Luppi M, Mantovani A, Velardi A, Romani L, Carvalho A. Genetic PTX3 deficiency and aspergillosis in stem-cell transplantation. *N Engl J Med* 2014;**370**:421–432.
35. Garlanda C, Hirsch E, Bozza S, Salustri A, De Acetis M, Nota R, Maccagno A, Riva F, Bottazzi B, Peri G, Doni A, Vago L, Botto M, De Santis R, Carminati P, Siracusa G, Altruda F, Vecchi A, Romani L, Mantovani A. Non-redundant role of the long pentraxin PTX3 in anti-fungal innate immune response. *Nature* 2002;**420**:182–186.
36. Knoflach M, Kiechl S, Mantovani A, Cuccovillo I, Bottazzi B, Xu Q, Xiao Q, Gasperi A, Mayr A, Kehrer M, Willeit J, Wick G. Pentraxin-3 as a marker of advanced atherosclerosis results from the Bruneck, ARMY and ARFY Studies. *PLoS One* 2012;**7**: e31474.
37. Baragetti A, Balzarotti G, Grigore L, Pellegatta F, Guerrini U, Pisano G, Fracanzani AL, Fargion S, Norata GD, Catapano AL. PCSK9 deficiency results in increased ectopic fat accumulation in experimental models and in humans. *Eur J Prev Cardiol* 2017; **24**:1870–1877.
38. Kloting N, M B. Adipocyte dysfunction, inflammation and metabolic syndrome. *Rev Endocr Metab Disord* 2014;**15**:277–287.
39. Murano I, Barbatelli G, Parisani V, Latini C, Muzzonigro G, Castellucci M, Cinti S. Dead adipocytes, detected as crown-like structures, are prevalent in visceral fat depots of genetically obese mice. *J Lipid Res* 2008;**49**:1562–1568.
40. Camozzi M, Rusnati M, Bugatti A, Bottazzi B, Mantovani A, Bastone A, Inforzato A, Vincenti S, Bracci L, Mastroianni D, Presta M. Identification of an antiangiogenic FGF2-binding site in the N terminus of the soluble pattern recognition receptor PTX3. *J Biol Chem* 2006;**281**:22605–22613.
41. Leali D, Inforzato A, Ronca R, Bianchi R, Belleri M, Coltrini D, Di Salle E, Sironi M, Norata GD, Bottazzi B, Garlanda C, Day AJ, Presta M. Long pentraxin 3/tumor necrosis factor-stimulated gene-6 interaction: a biological rheostat for fibroblast growth factor 2-mediated angiogenesis. *Arterioscler Thromb Vasc Biol* 2012;**32**:696–703.
42. Mathis D. Immunological goings-on in visceral adipose tissue. *Cell Metab* 2013;**17**: 851–859.
43. Woolford SJ, Clark SJ, Lumeng JC, Williams DR, Davis MM. Maternal perspectives on growth and nutrition counseling provided at preschool well-child visits. *J Natl Med Assoc* 2007;**99**:153–158.
44. Mauro C, Smith J, Cucchi D, Coe D, Fu H, Bonacina F, Baragetti A, Cermenati G, Caruso D, Mitro N, Catapano AL, Ammirati E, Longhi MP, Okkenhaug K, Norata GD, Marelli-Berg FM. Obesity-induced metabolic stress leads to biased effector memory CD4(+) T cell differentiation via PI3K p110delta-Akt-mediated signals. *Cell Metab* 2017;**25**:593–609.
45. Kanda H, Tateya S, Tamori Y, Kotani K, Hiasa K, Kitazawa R, Kitazawa S, Miyachi H, Maeda S, Egashira K, Kasuga M. MCP-1 contributes to macrophage infiltration into adipose tissue, insulin resistance, and hepatic steatosis in obesity. *J Clin Invest* 2006; **116**:1494–1505.
46. Chatzigeorgiou A, Seijkens T, Zarzycka B, Engel D, Poggi M, van den Berg S, van den Berg S, Soehnlein O, Winkels H, Beckers L, Lievens D, Driessen A, Kusters P, Biessen E, Garcia-Martin R, Klotzsche-von Ameln A, Gijbels M, Noelle R, Boon L, Hackeng T, Schulte K-M, Schulte K, Xu A, Vriend G, Nabuurs S, Chung K-J, Willems van Dijk K, Rensen PCN, Gerdes N, de Winther M, Block NL, Schally AV, Weber C, Bornstein SR, Nicolaes G, Chavakis T, Lutgens E. Blocking CD40-TRAF6 signaling is a therapeutic target in obesity-associated insulin resistance. *Proc Natl Acad Sci USA* 2014;**111**:2686–2691.
47. Doni A, Musso T, Morone D, Bastone A, Zambelli V, Sironi M, Castagnoli C, Cambieri I, Stravalaci M, Pasqualini F, Laface I, Valentino S, Tartari S, Ponzetta A, Maina V, Barbieri SS, Tremoli E, Catapano AL, Norata GD, Bottazzi B, Garlanda C, Mantovani A. An acidic microenvironment sets the humoral pattern recognition molecule PTX3 in a tissue repair mode. *J Exp Med* 2015;**212**:905–925.
48. Bonavita E, Gentile S, Rubino M, Maina V, Papait R, Kunderfranco P, Greco C, Feruglio F, Molgora M, Laface I, Tartari S, Doni A, Pasqualini F, Barbati E, Basso G, Galdiero MR, Nebuloni M, Roncalli M, Colombo P, Laghi L, Lambris JD, Jaillon S, Garlanda C, Mantovani A. PTX3 is an extrinsic oncosuppressor regulating complement-dependent inflammation in cancer. *Cell* 2015;**160**:700–714.
49. Souza DG, Amaral FA, Fagundes CT, Coelho FM, Arantes RM, Sousa LP, Matzuk MM, Garlanda C, Mantovani A, Dias AA, Teixeira MM. The long pentraxin PTX3 is crucial for tissue inflammation after intestinal ischemia and reperfusion in mice. *Am J Pathol* 2009;**174**:1309–1318.
50. Inforzato A, Reading PC, Barbati E, Bottazzi B, Garlanda C, Mantovani A. The "sweet" side of a long pentraxin: how glycosylation affects PTX3 functions in innate immunity and inflammation. *Front Immunol* 2012;**3**:407.
51. Moreno PR, Purushothaman KR, Sirol M, Levy AP, Fuster V. Neovascularization in human atherosclerosis. *Circulation* 2006;**113**:2245–2252.
52. Sung HK, Doh KO, Son JE, Park JG, Bae Y, Choi S, Nelson SM, Cowling R, Nagy K, Michael IP, Koh GY, Adamson SL, Pawson T, Nagy A. Adipose vascular endothelial growth factor regulates metabolic homeostasis through angiogenesis. *Cell Metab* 2013;**17**:61–72.
53. Cao Y. Angiogenesis modulates adipogenesis and obesity. *J Clin Invest* 2007;**117**: 2362–2368.
54. Elias I, Franckhauser S, Ferre T, Vila L, Tafuro S, Munoz S, Roca C, Ramos D, Pujol A, Riu E, Ruberte J, Bosch F. Adipose tissue overexpression of vascular endothelial growth factor protects against diet-induced obesity and insulin resistance. *Diabetes* 2012;**61**:1801–1813.
55. Kim KH, Kim YH, Son JE, Lee JH, Kim S, Choe MS, Moon JH, Zhong J, Fu K, Lenglin F, Yoo JA, Bilan PJ, Klip A, Nagy A, Kim JR, Park JG, Hussein SM, Doh KO, Hui CC, Sung HK. Intermittent fasting promotes adipose thermogenesis and metabolic homeostasis via VEGF-mediated alternative activation of macrophage. *Cell Res* 2017;**27**: 1309–1326.
56. Odegaard JI, Ricardo-Gonzalez RR, Goforth MH, Morel CR, Subramanian V, Mukundan L, Red Eagle A, Vats D, Brombacher F, Ferrante AW, Chawla A. Macrophage-specific PPARgamma controls alternative activation and improves insulin resistance. *Nature* 2007;**447**:1116–1120.
57. Nauta AJ, Bottazzi B, Mantovani A, Salvatori G, Kishore U, Schwaeble WJ, Gingras AR, Tzima S, Vivanco F, Egido J, Tijsma O, Hack EC, Daha MR, Roos A. Biochemical and functional characterization of the interaction between pentraxin 3 and C1q. *Eur J Immunol* 2003;**33**:465–473.
58. Ho MM, Manughian-Peter A, Spivia WR, Taylor A, Fraser DA. Macrophage molecular signaling and inflammatory responses during ingestion of atherogenic lipoproteins are modulated by complement protein C1q. *Atherosclerosis* 2016;**253**:38–46.